Eur. Phys. J. AP **6**, 23–31 (1999)

THE EUROPEAN PHYSICAL JOURNAL APPLIED PHYSICS

Dielectric properties of periodic heterostructures: A computational electrostatics approach*

C. Brosseau[1,a] and A. Beroual[2,b]

[1] Laboratoire d'Électronique et Systèmes de Télécommunications, Université de Bretagne Occidentale, 6 avenue Le Gorgeu, B.P. 809, 29285 Brest Cedex, France

[2] Centre de Génie Électrique de Lyon, École Centrale de Lyon, B.P. 163, 36 avenue Guy de Collongue, 69131 Écully Cedex, France

Received: 10 August 1998 / Revised: 13 October 1998 / Accepted: 17 December 1998

Abstract. The dielectric properties of heterogeneous materials for various condensed-matter systems are important for several technologies, *e.g.* impregnated polymers for high-density capacitors, polymer carbon black mixtures for automotive tires and current limiters in circuit protection. These multiscale systems lead to challenging problems of connecting microstructural features (shape, spatial arrangement and size distribution of inclusions) to macroscopic materials response (permittivity, conductivity). In this paper, we briefly discuss an *ab initio* computational electrostatics approach, based either on the use of the field calculation package FLUX3D (or FLUX2D) and a conventional finite elements method, or the use of the field calculation package PHI3D and the resolution of boundary integral equations, for calculating the effective permittivity of two-component dielectric heterostructures. Numerical results concerning inclusions of permittivity ε_1 with various geometrical shapes periodically arranged in a host matrix of permittivity ε_2 are provided. Next we discuss these results in terms of phenomenological mixing laws, analytical theory and connectedness. During the pursuit of these activities, several interesting phenomena were discovered that will stimulate further investigation.

PACS. 77.22.Ch Permittivity (dielectric function) – 02.70.Dh Finite-element and Galerkin methods – 41.20.Cv Electrostatics; Poisson and Laplace equations, boundary-value problems

1 Introduction

In recent years the dielectric properties of disordered heterogeneous materials have received considerable fundamental attention and these investigations continue to be centrally important for developing a deeper understanding leading to innovative technological applications in the areas of electronics, automotive tires and aerospace industries, to cite but a few. The everincreasing need for devices capable of operating at high power levels, high frequencies, high temperatures and chemically hostile environments is driving researchers to develop composite materials which are capable to overcome these technological challenges.

A wide variety of processes lead to intricate condensed-matter heterostructures having complex morphologies. However many of them show striking similarities: the issue of connectedness has emerged as a key element to our understanding of the electrical properties of heterostructures, such as colloidal dispersions, granular materials, metal-insulator films, and many others [1–5]. A fundamental question is whether these diverse systems are described by the same physics. In recent years some progress has been made toward answering this question by means of experiment, analytical theories and computer simulations. It goes without saying that there are a number of systems of practical interest where the answer to this question could find technological applications, *e.g.* impregnated polymers (*e.g.* polypropylene) for high-density capacitors [6], and polymer carbon black mixtures for automotive tires and current limiters [7,8]. Each individual system is of course unique unto itself but, consistent with this diversity, there are overall similarities which one would like to explain. Numerical simulation indicates that one can in fact explain at least partially many of the observed features by simply considering a quasistatic approach, ignoring altogether the details of the microstructure, and any other complications, *e.g.* aggregation structure, adsorption and porosity effects. This suggests that the observed dielectric characteristics should be described almost completely by quasiuniversal laws [9]. In this work we address this question through a series of numerical simulations.

* This paper was presented at the PIERS 98 conference (Progress in Electromagnetics Research Symposium) held at Nantes (France), July 13-17, 1998.

[a] e-mail: brosseau@univ-brest.fr

[b] e-mail: beroual@trotek.ec-lyon.fr

The work stems from earlier extensive studies in which we used the finite elements method and boundary integral equations to calculate the complex effective permittivity of a two component heterostructure as a function of volume (or area) fraction, shapes, sizes and distribution in space (or surface) of the inclusions [10–13]. There are at least two important aspects that contribute to the reliability and versatility of these simulation methods. On the one hand, they are first principles approaches which give quantitative results over the entire range of component concentration. These methods are exact in principle for regular arrays forming a crystal lattice because they include all the relevant physical effects, *i.e.* multipole polarizabilities. On the other hand, these calculational methods are not computationally intensive and they will yield the effective permittivity to the accuracy implied by a finite-size simulation of an infinite material.

The primary purpose of this paper is to discuss two *ab initio* numerical studies of the complex effective permittivity of a two component periodic composite material. The secondary purpose is to present quantitative but illustrative computations of macroscopic dielectric properties of such systems and show that many of the experimental features are captured well.

Briefly, this paper is organized as follows. We first outline the basic computational framework in terms of which the problem of evaluating the dielectric properties of systems of regular objects, *e.g.* cubes, spheres and ellipsoids, can be approached. Then we illustrate concretely how the permittivity of such materials depends on three factors: the dielectric properties of the constituents, their volume (or area) fractions and the way in which they are arranged. We find interesting to discuss these results in terms of phenomenological mixing laws, analytical theory and connectedness. The paper ends with a discussion of several future directions for continuing the development of the research.

2 Numerical simulation

The complex effective dielectric constant, relative to free space, $\varepsilon = \varepsilon' - \mathrm{i}\varepsilon''$ carries information about the average polarization in the heterogeneous medium and is defined as the ratio of the average displacement field vector and the applied electric field. We may write this quantity as

$$\overline{E}^2 \varepsilon = \frac{1}{\Omega} \int_\Omega \hat{\varepsilon} |\nabla V|^2 \mathrm{d}\Omega,$$

where $\hat{\varepsilon}$ is a spatially dependent permittivity, $\overline{E} = (1/\Omega) \int_\Omega E \, \mathrm{d}\Omega$ denotes a volume average field over a sample large compared with microscopic correlation lengths and depends on the applied potentials, E is the local electric field in the cell and Ω is the volume of the medium. The absolute complex dielectric constant is obtained by multiplying ε by the permittivity of free space ε_0. Here the imaginary part ε'' is due to the absorption since scattering attenuation is assumed negligible. The complex effective permittivity will depend on the permittivity of each constituent in the mixture, their volume (or area) fractions and eventually on the sizes, shapes and distribution in space (or surface) of the inclusions.

For simplicity we will consider a composite medium made up of two nonmagnetic (we take $\mu_1 = \mu_2 = 1$) materials with relative dielectric constants $\varepsilon_1 = \varepsilon_1' - i\varepsilon_1''$ and $\varepsilon_2 = \varepsilon_2'$. We denote by f the concentration occupied by the inclusions of permittivity ε_1 periodically placed within the host material (continuum) with permittivity ε_2. When considering the propagation of an electromagnetic wave in heterogeneous media, two length scales are of importance. The first scale is the wavelength λ of the wave probing the medium. The second one is the typical size ξ of the inhomogeneities. When the two conditions $k_1 \xi \ll 1$ and $k_2 \xi \ll 1$ are met, where we have set:

$$k_i = (\varepsilon_i \mu_i)^{\frac{1}{2}} \frac{2\pi}{\lambda} \quad i = 1, 2,$$

the wave cannot resolve the individual scatterers and thus the material appears homogeneous to the probing wave. In this quasistatic limit, the system can be described by an effective (average) dielectric constant ε which is a linear homogeneous function of ε_1 and ε_2.

Many experimental observations in dielectric heterostructures are commonly fit with phenomenological mixing laws, *e.g.* the Maxwell Garnett rule [1]. The main difficulties, to which we return below, are that mixing formulas all give more or less the same results at low concentration of inclusions (dilute limit) and that mixing laws cannot realistically describe the percolation threshold, but there are many others. Such difficulties are extensively surveyed in several review articles [1,4,5].

The calculation of the effective dielectric constant of composite materials from the known properties of the pure, homogeneous components, is an electrostatics problem which involves the resolution of partial differential equations and taking into account boundary conditions defined on domains with given geometries. Here we give only some of the most important details of the model investigated and the essential features of the simulation. More details can be found elsewhere [10–13]. The solution of Laplace's equation can be computed by applying either the method of boundary integral equation (BIE) using the field calculation package PHI3D, or the finite elements (FE) method using the field calculation packages FLUX3D for three-dimensional systems and FLUX2D for two-dimensional systems of various objects. We describe below these two simulation procedures and examine their differences.

2.1 PHI3D and BIE

We start from the first principles in electrostatics, namely Laplace's equation, *i.e.* $\nabla(\varepsilon \nabla V) = 0$, where V is a potential distribution inside a spatial domain Ω with a density of charge equals to zero everywhere. Upon using Green's theorem, we can write the local potential $V(M \in \Omega)$ in

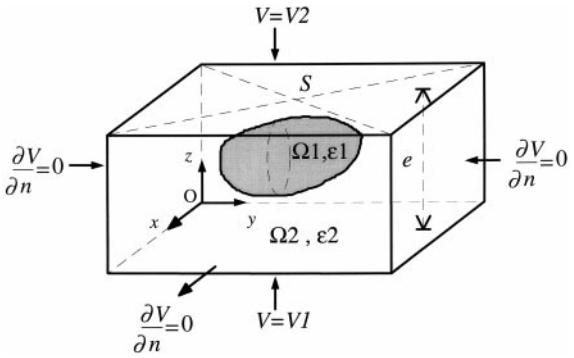

Fig. 1. A schematic diagram of the unit cell of the two-component periodic composite (three-dimensional) material investigated in the numerical computation. The isolated inclusion with dielectric constant ε_1 is periodically arranged in a three-dimensional structure. The dielectric constant of the remaining space is ε_2. See text for notations. This configuration corresponds to low concentrations of inclusions.

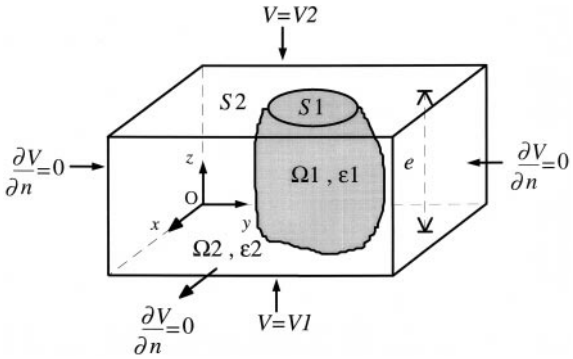

Fig. 2. Same as in Figure 1 for a fused inclusion with dielectric constant ε_1. This configuration corresponds to high concentrations of inclusions.

terms of $V(P)$ and of the normal derivative $\partial V(P)/\partial n$, with P being any point on the boundary Σ (with no overhangs) of Ω:

$$V(M) = -\frac{4\pi}{A}\int_{\Sigma}\left(V(P)\frac{\partial G}{\partial n} - G\frac{\partial V(P)}{\partial n}\right)\mathrm{d}s, \qquad (1)$$

where A stands for the solid angle under which the point M sees the oriented surface Σ, n is the normal unit vector oriented outward to $\Sigma, \mathrm{d}s$ is a surface element of Σ and G denotes the Green function. As an illustration displayed in Figure 1, we have represented an arbitrarily shaped homogeneous inclusion occupying a volume Ω_1 and permittivity ε_1, which is embedded in a homogeneous matrix of volume Ω_2 and permittivity ε_2. Absence of charge density is tacitly assumed through the analysis. given these assumptions, equation (1) leads to

$$V = -\frac{4\pi}{A}\int_{\Sigma_1}\left(V\frac{\partial G}{\partial n} - G\left(\frac{\partial V}{\partial n}\right)_1\right)\mathrm{d}s, \qquad (2)$$

for domain 1, and

$$V = -\frac{4\pi}{A}\int_{\Sigma_2}\left(V\frac{\partial G}{\partial n} - G\left(\frac{\partial V}{\partial n}\right)_2\right)\mathrm{d}s \qquad (3)$$

for domain 2. Moreover, we have

$$\varepsilon_1\left(\frac{\partial V}{\partial n}\right)_1 = \varepsilon_2\left(\frac{\partial V}{\partial n}\right)_2, \qquad (4)$$

by virtue of the conservation of the normal component of the electric displacement vector at the interface. Consequently, we have to solve the above two integral equations (2, 3) to evaluate numerically the electrostatic potential distribution. For that purpose, the implementation of the BIE method consists in dividing the boundaries into FE and for each FE, the calculation is carried out by interpolation of V and $\partial V/\partial n$ with the corresponding nodal values $V = \sum_j \lambda_j V_j$ and $\partial V/\partial n = \sum_j \lambda_j \left(\partial V/\partial n\right)_j$, where λ_j denote interpolating functions [14]. Consequently only the surface bounding the volume is meshed. Following this way, integral equations are transformed in a matrix equation which is numerically solved using the boundary conditions on each side of the unit cell as displayed in Figure 1. The total polarization of the configuration of inclusions is then available by matrix algebra. In Figure 1, the inclusion is isolated (low concentration) and thus the medium of permittivity ε_1 cannot intercept the sides of the parallelipipedic cell. In that case, the effective permittivity, in the direction corresponding to the applied field, is calculated using the following relation

$$\int_S \varepsilon_2\left(\frac{\partial V}{\partial n}\right)_2 = \varepsilon\frac{V_2 - V_1}{e}S, \qquad (5a)$$

where $V_2 - V_1$ denotes the difference of potential imposed in the z-direction, e is the composite thickness in the same direction and S is the surface of the unit cell perpendicular to the applied field (see Fig. 1). If the inclusions are allowed to fuse each other (high concentration regime), the region of permittivity ε_1 can intercept the sides of the parallelipipedic cell (see Fig. 2). In that case, we have to take into account the electric displacement flux through the area S_1 for the calculation of the effective permittivity in the direction corresponding to the applied field [10]. Then, equation (5a) needs to be changed in

$$\int_{S_2}\varepsilon_2\left(\frac{\partial V}{\partial n}\right)_2 + \int_{S_1}\varepsilon_1\left(\frac{\partial V}{\partial n}\right)_1 = \varepsilon\frac{V_2 - V_1}{e}(S_1 + S_2). \qquad (5b)$$

To close this section, it should be noted that the BIE method gives an accurate description of the electric potential by taking into account edge and proximity effects even for a high concentration of inhomogeneities. Therefore, this numerical value does not suffer from the disadvantages of the traditional boundary-value approach.

2.2 FLUX3D (or FLUX 2D) and FE

All the procedural details for three-dimensional and two-dimensional systems can be found in previous work

[10–12]. We now briefly develop the method for three-dimensional systems. The procedure can be extended easily for the two-dimensional case [11]. Its numerical implementation consists in dividing the volume domain into tetrahedral finite elements and for each element, the calculation is carried out by interpolation of the potential V and its normal derivative $\partial V/\partial n$ with the corresponding nodal values $V = \sum_j \lambda_j V_j$ and $\partial V/\partial n = \sum_j \lambda_j \left(\partial V/\partial n\right)_j$, where λ_j denote interpolating functions [14]. The field and potential distributions are obtained from the boundary conditions using the Galerkin method and solving the matrix equations resulting from the discretization procedure by standard numerical techniques, *e.g.* Gauss method [15]. Having computed the potential and its normal derivative on each node of the mesh, the electrostatic energy

$$\delta W_{\mathrm{e}}(k) = \frac{1}{2}\int_{V_k}\iint \varepsilon'_k \left[\left(\frac{\partial V}{\partial x}\right)^2 + \left(\frac{\partial V}{\partial y}\right)^2 + \left(\frac{\partial V}{\partial z}\right)^2\right] \mathrm{d}x\mathrm{d}y\mathrm{d}z,$$

for each tetrahedral element is evaluated, where ε'_k and v_k denote the real part of the permittivity and the surface of the kth element respectively. Thus the total energy of the entire composite can be written by summation over the n_k elements such as $W_{\mathrm{e}} = \sum_{k=1}^{n_k} \delta W_{\mathrm{e}}(k)$. In the problem at hand, we consider a portion of the composite material which is the filler of a parallel plate capacitor. In this manner we obtain the real part of the complex effective permittivity from the electrostatic energy stored in such a capacitor, *i.e.* $W_{\mathrm{e}} = (1/2)\varepsilon'(S_{\mathrm{d}}/e)(V_2 - V_1)^2$ when a given potential difference is applied across the plates (see Fig. 1), $S_{\mathrm{d}} = Ld$ stands for the surface of the plates with side of length L (for the two-dimensional structures considered below, we shall take $d = 1$ unit of length). Now, we must relate the dielectric losses to the imaginary part of ε. To do so, the dielectric losses are evaluated on each element of the mesh as

$$\delta\rho(k) = \frac{1}{2}\int_{V_k}\iint \omega\varepsilon'_k \tan\delta_k \left[\left(\frac{\partial V}{\partial x}\right)^2 + \left(\frac{\partial V}{\partial y}\right)^2 + \left(\frac{\partial V}{\partial z}\right)^2\right] \mathrm{d}x\mathrm{d}y\mathrm{d}z,$$

where $\tan\delta_k$ is the loss tangent of the kth element and ω is the angular frequency of the electric field. The total losses of the entire composite is then obtained by summation over the n_k elements such as $\rho = \sum_{k=1}^{n_k} \delta\rho(k)$ and finally its connection with the imaginary part of the complex effective permittivity is $\rho = (1/2)\varepsilon''(S_{\mathrm{d}}/e)\omega(V_2 - V_1)^2$. To test the validity of the computational procedure we have compared on numerical simulation with many analytical procedures [10,11].

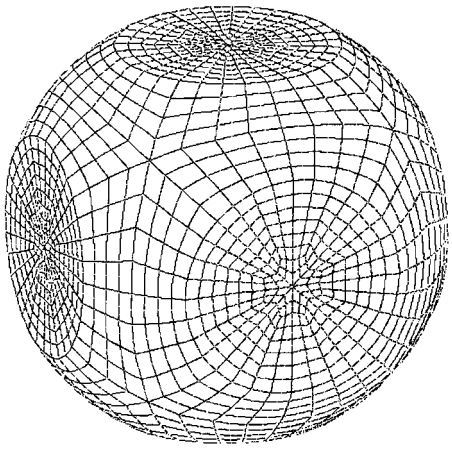

Fig. 3. A computational mesh of the spherical inclusion in the unit cell of the composite beyond the touching sphere condition.

2.3 Differences between PHI3D and FE methods

This subsection is devoted to examining several differences between the two above outlined computational approaches. The FE method can be used either for treating linear and nonlinear problems, however it is less appropriate than the BIE method for treating open problems [14]. By contrast, the BIE method is relevant to study open and closed problems, but is not appropriate to nonlinear problems [14]. One salient feature of the BIE method is that only the boundaries of the geometry need be discretized which has for effect to reduce the memory space required for manipulation of data, but the matrix equation to solve is asymmetric and full. By contrast the corresponding matrix equation obtained by the FE method is sparse. One can use standard iterative methods to solve the matrix equation within the BIE method while, in the FE formulation, one should use other methods, *e.g.* Gauss triangulation, that induce a limitation of this method because CPU time increases as the cube of the number of unknown quantities. Next we observe that the field calculation package FLUX 3D uses an automatic meshing system based upon the Delaunay's approach while the field calculation package PHI3D considers a semi-automatic meshing system [14,15]. Finally we note that the computational time to run our simulations on a HP model 712/80 workstation are linked with the details of the meshing of the geometry considered and ranges from a few minutes to a few hours for calculating the permittivity of a typical three-dimensional configuration. From the standpoint of computational time the two methods are equivalent. Finally it is noted that we compared the numerical results for a series of geometrical configurations. For example, test cases concerning spherical inclusions ($\varepsilon_1 = 80 - \mathrm{i}10^x$, with $-1 < x < 3$ arranged in a simple-cubic lattice in a host matrix ($\varepsilon_2 = 2 - \mathrm{i}0$) have given similar results of the real and imaginary parts of the effective permittivity. More details can be found in the appropriate publications [10–13].

With these considerations in mind, we now turn to the presentation of the results of our numerical experiments.

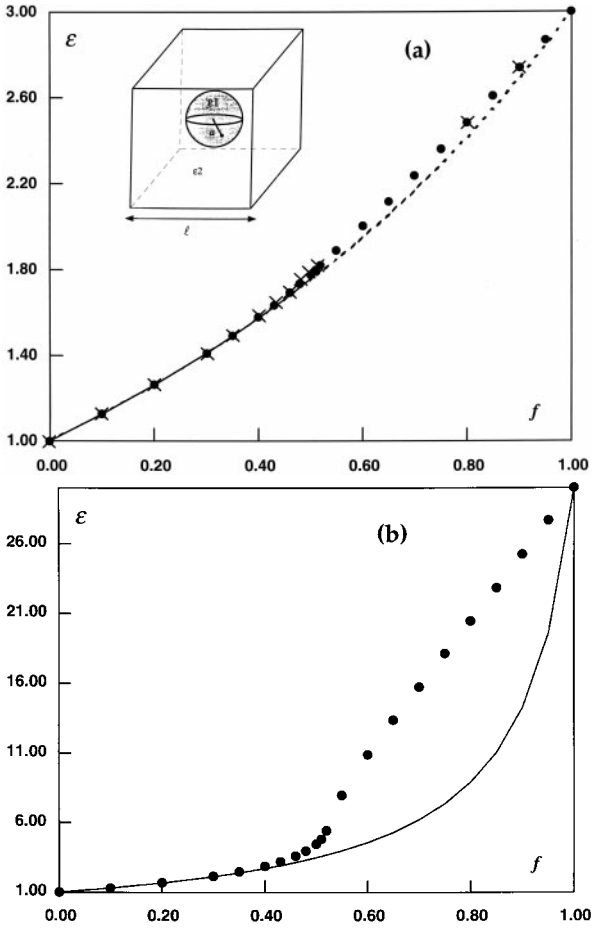

Fig. 4. (a) Volume fraction dependence of the effective permittivity of the three-dimensional periodic composite composed of spherical inclusions (permittivity $\varepsilon_1 = 3$) of volume fraction f placed in a host matrix (permittivity $\varepsilon_2 = 1$). The inset shows the configuration studied. The full circles are obtained by the FE method. The solid line is obtained from the results of McPhedran *et al.* [16]. Crosses are results of Tao *et al.* [17]. The dashed curve corresponds to the Maxwell Garnett equation. (b) Same as in (a) for $\varepsilon_1 = 30$ and $\varepsilon_2 = 1$.

3 Numerical results and discussion

In this section we systematically go through the dielectric properties of two component regular heterostructures and analyze how they are related to the spatial arrangement and inclusions shape.

3.1 Spherical, ellipsoidal and cubic inclusions arranged in a three-dimensional simple-cubic lattice

Using the numerical simulation method based on FLUX3D and FE, we have first evaluated the effective permittivity of a simple cubic lattice arrangement of monodisperse spheres. The results for ε as a function of the volume fraction f are shown in Figures 4a and 4b. We have set $\varepsilon_1 = 3$ and $\varepsilon_2 = 1$ in Figure 2a and $\varepsilon_1 = 30$ and $\varepsilon_2 = 1$ in Figure 4b. In Figure 4a, we have compared our results with those derived from Maxwell Garnett mixing law and those obtained by McPhedran *et al.* [16] and Tao *et al.* [17]. In that case, it appears that the value of ε computed by our numerical method agrees satisfactorily with these previous calculations. It is also interesting to observe the limits of the Maxwell Garnett theory for volume fractions f above $\cong 0.5$, as the ratio $\varepsilon_1/\varepsilon_2$ is increased (Fig. 4b). Note that this value is very close to the maximum packing density, *i.e.* when the spheres make contact, of a suspension of nonoverlapping spheres of equal size which is $f_{\rm p} = 0.52$ for a simple cubic lattice. The deviation from Maxwell Garnett mixing law is a macroscopic manifestation of the nonlinear dependence of the higher multipolar interactions on the distances between the inclusions. This deviation is more and more visible when the ratio $\varepsilon_1/\varepsilon_2$ is increased.

Next Figures 5a and 5b show the numerical values for permittivity of ellipsoids periodically arranged in a simple cubic lattice at various volume fractions. Figures 5a and 5b show a comparison of our simulational data for the effective permittivity of the medium in the x- and z-directions respectively ($\varepsilon_1 = 30$ and $\varepsilon_2 = 1$) and those obtained with the mean-field formula given by Sihvola and Kong [18]

$$\varepsilon_i = \varepsilon_2 \left(1 + \frac{(\varepsilon_1 - \varepsilon_2) f}{\varepsilon_2 + (\varepsilon_1 - \varepsilon_2)(1 - f) L_i} \right) \qquad i = x,\ y,\ z, \quad (6)$$

where $f = (4\pi/3)(abc/lwh)$ is the volume fraction of the constituent 1 (see the inset of Fig. 5a) and L_i is the depolarization factor in the direction characterized by the index i. To simplify further the analysis, we choose $b = c = a/2$ (prolate ellipsoid) and we take the dimensions of the elementary cell such $l = 4$ and $w = h = 2$. Significant deviations from these numerical simulations with equation (6) can be observed for $f \geq f_{\rm p}$, the effect being more important in the x-direction for which the interaction effects are stronger.

We turn now to a three-dimensional simple cubic lattice arrangement of cubic inclusions. Figures 6a and 6b show the comparison of numerical results provided by our simulation with Maxwell Garnett equation for two values of the ratio $\varepsilon_1/\varepsilon_2$ of permittivities. We remark that the agreement of the numerical data with Maxwell Garnett law is good. The difference with the previous cases comes from the fact that equal-sized spheres and ellipsoids cannot fill space but cubes can.

In general any approach based only on the dipole approximation must fail to correctly describe the permittivity over the entire range of volume loading [1,4]. Mean-field theories neglect the correlations among the inclusions that become important when the system is not dilute and the contrast between the components, *i.e.* $\varepsilon_1/\varepsilon_2$, is very different from 1. High-order multipole interactions become important when the particles approach contact and are taken into account exactly in our numerical experiments. Therefore these results can be used as a benchmark to check the validity of the available empirical formulas or

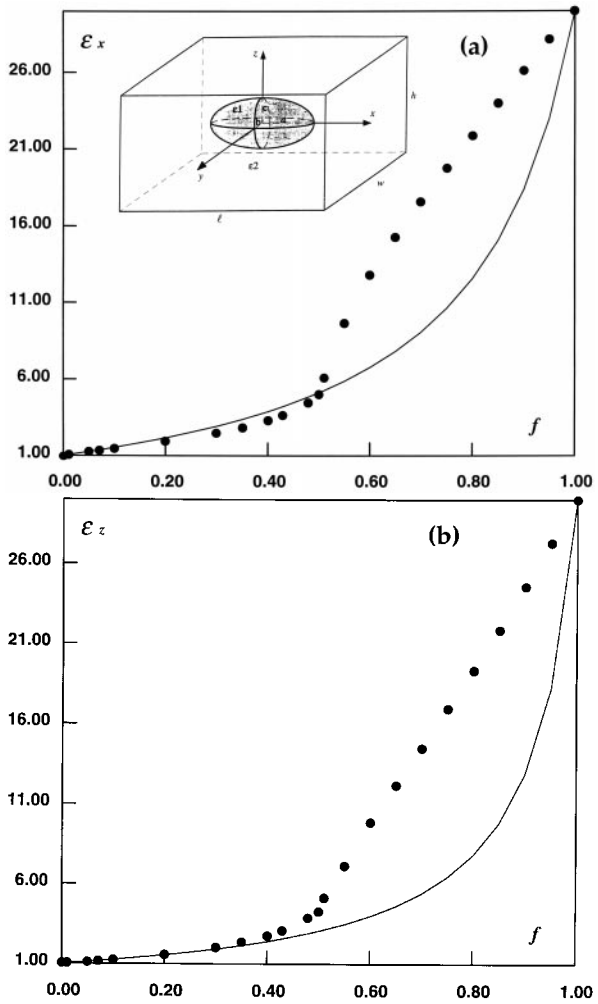

Fig. 5. (a) The effective permittivity in the x-direction (solid circle) is shown as a function of the volume fraction f of the inclusion phase. Ellipsoidal inclusions ($b = c = a/2$) of permittivity $\varepsilon_1 = 30$ are placed in a host matrix material of permittivity $\varepsilon_2 = 1$. The inset shows the configuration studied. Simple cubic lattice. The solid line shown in this figure corresponds to results obtained from equation (6) with a depolarization factor $L_x = 0.1736$. (b) Same as in (a) for the effective permittivity in the z-direction. The solid line shown in this figure corresponds to results obtained from equation (6) with a depolarization factor $L_z = 0.4132$.

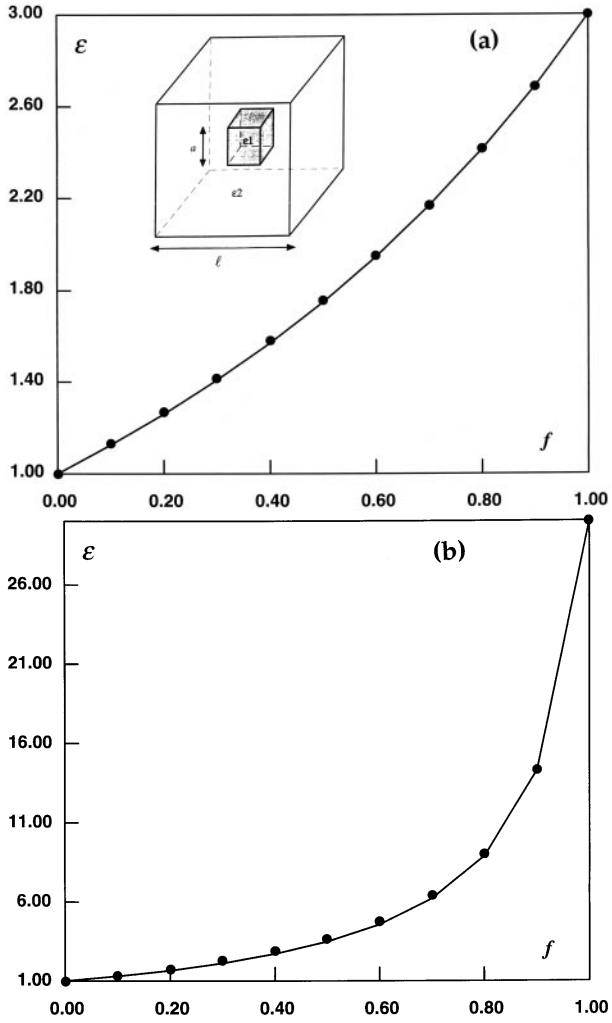

Fig. 6. (a) The effective permittivity (solid circle) is shown as a function of the volume fraction f of the inclusion phase. Cubic inclusions (permittivity $\varepsilon_1 = 3$) are placed in a host matrix material of permittivity $\varepsilon_2 = 1$. The inset shows the configuration studied. Simple cubic lattice. The solid line shown in this figure corresponds to results obtained from Maxwell Garnett equation. (b) Same as in (a) for $\varepsilon_1 = 30$ and $\varepsilon_2 = 1$.

theoretical calculations that have been proposed to evaluate the effective permittivity of heterostructures.

3.2 Discoidal inclusions arranged in a two-dimensional simple-square lattice

In this section, we present a numerical study of a two-dimensional square array of inclusions based on FLUX2D and FE. Let us consider the details of Figure 7 with Cartesian spatial coordinates x, y and z. This figure represents the axisymmetric unit cell of the two-component structure under study. It has been chosen for purpose of comparison with the results of Liu and Shen [19]. The structure

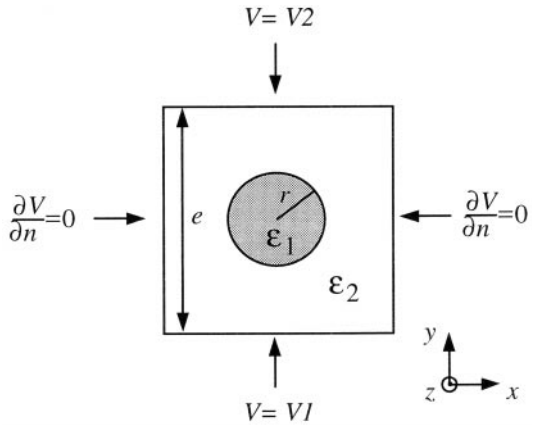

Fig. 7. Unit cell of a simple square lattice of identical discoidal inclusions with permittivity ε_1 embedded in a host material with permittivity ε_2.

consists of an infinite circular cylinder (ε_1) of radius r and with generator parallel to the z axis embedded in a host matrix (ε_2), *i.e.* the intersections of the cylinders with the xy plane form a periodic two-dimensional structure (simple square lattice of side $e = 1$). This symmetrical structure in both the x and y directions renders the two-component composite material to be both translationally and rotationally invariant. We denote by f the fractional occupancy of constituent 1: $f = \pi r^2$ below the non-overlapping concentration ($0 \leq r \leq 1/2$), and

$$f = \pi r^2 - 4r^2 \arccos\left(\frac{1}{r}\right) + \sqrt{4r^2 - 1}$$

beyond the non-overlapping concentration ($1/2 \leq r \leq 1/\sqrt{2}$). The $r \geq 1/2$ case is special because the symmetry of the structure provides that we can exclude in our numerical calculations the four sections of the component of permittivity ε_1 exceeding from the unit square cell.

To facilitate the comparison with the results of [20,21], we first use the following set of parameters: $\varepsilon_1 = 1-3\mathrm{i}$ and $\varepsilon_2 = 5-8\mathrm{i}$. In Figure 8 we show a comparison of the effective permittivity computed for the two-pole approximation (Bergman-Milton theory [20,21]) and the FE method versus the radius of the circular cylinder. Figures 8a and 8b are for the real part and imaginary part of ε respectively. As can be recognized from these figures, in the range of r investigated, the values of the effective complex permittivity obtained from the Bergman-Milton theory are quantitatively very similar to the ones presented in this work. The only thing that changes is that the values of ε' and ε'' are slightly higher than those given by the 2-pole approximation. These data confirm the usefulness of the FE algorithm as an efficient tool for computing the complex effective permittivity of lossy composite media. Liu and Shen's method is based on a Fourier expansion technique which is costly in computer time even in the two-dimensional case considered here. By contrast, our method is not time consuming. The CPU time for calculating the permittivity of a typical two-dimensional configuration is of the order of a few seconds.

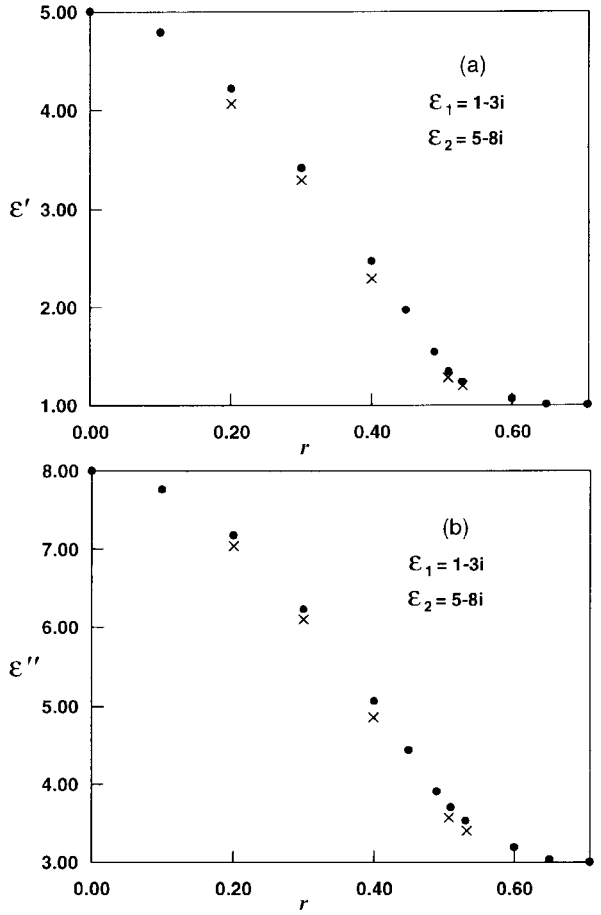

Fig. 8. (a) Comparison of the real part of the complex effective dielectric constant evaluated by the finite-element method (•) and the 2-pole Bergman-Milton approximation (×, Ref. [19]) as a function of the radius of the circular cylinder r. The dielectric constants of the two-component composite material are $\varepsilon_1 = 1-3\mathrm{i}$ and $\varepsilon_2 = 5-8\mathrm{i}$. (b) Same as in (a) for the imaginary part of the complex effective dielectric constant.

3.3 Rodlike inclusions arranged in a three-dimensional simple-cubic lattice

To illustrate the predictions of the BIE method using the field calculation package we consider rodlike inclusions arranged in a simple-cubic lattice. In the numerical experiments that follow we assume that $\varepsilon_1 = 80 - \mathrm{i}10^2$ and $\varepsilon_2 = 2 - \mathrm{i}0$. The unit cell of the heterostructure we consider is reproduced in the inset of Figure 9a. More specifically, the rod radius r (in dimensionless units) is kept fixed and the volume fraction of the inclusions changes by varying the rod length l. In Figures 9a and 9b we display the real and imaginary parts of the permittivity in the z direction as function of concentration and various radius-to-length ratios r/l, for 6 values of r ranging from 0.05 to 0.45. Note that as r is increased, the maximum packing density, *i.e.* when the rodlike inclusions make contact, shifts to a higher concentration. We have also observed that, due to the shape anisotropy of the inclusions, this transition is much sharper than for spheres [22].

A related issue is how the orientation of the rod axis with respect to the direction of the applied electric field, *i.e.* the z-axis, affects the effective permittivity. Numerical results for oriented inclusions with an angle $\alpha = 30^\circ$ are shown in Figures 10a and 10b. In Figure 10a (resp. Fig. 10b) we plot in a log-log plot the real (resp. imaginary) part of the effective permittivity for 4 different radii of the rodlike inclusions. One interesting aspects of Figures 10a and 10b is that, for a given volume fraction of the inclusions, the real and imaginary parts of the effective permittivity decrease as the angle of orientation α increases.

This behavior we believe to reflect the connectedness, *i.e.* the ability the inclusions have in making contact with each other. Spherical shape provides a minimum of surface area for a given volume of material and a fixed number of inclusions. This is also consistent with the fact that, for a

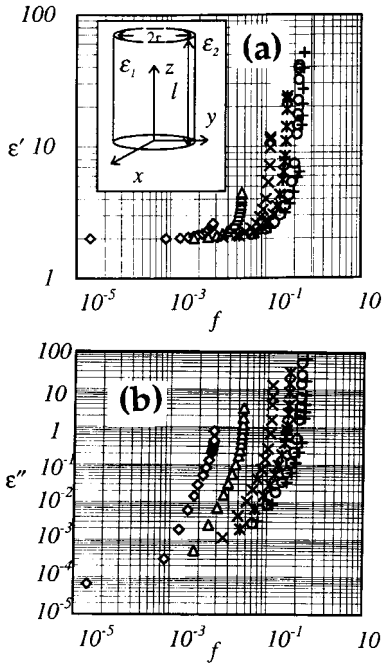

Fig. 9. (a) The real part of the effective permittivity ε_z' is shown as a function of the volume fraction f of the inclusion phase. Rodlike inclusions (permittivity $\varepsilon_1 = 80 - \mathrm{i}10^2$) are placed in a host matrix material of permittivity $\varepsilon_2 = 2 - \mathrm{i}0$. Simple-cubic lattice configuration. The inset shows the configuration of the two-component periodic composite material investigated in this study. ($\Diamond$) $r = 0.05$, ($\triangle$) $r = 0.10$, ($\times$) $r = 0.20$, ($*$) $r = 0.30$, ($\circ$) $r = 0.40$, ($+$) $r = 0.45$. The solid lines are guides to the eye. (b) Same as in (a) for the imaginary part of the effective permittivity ε_z''.

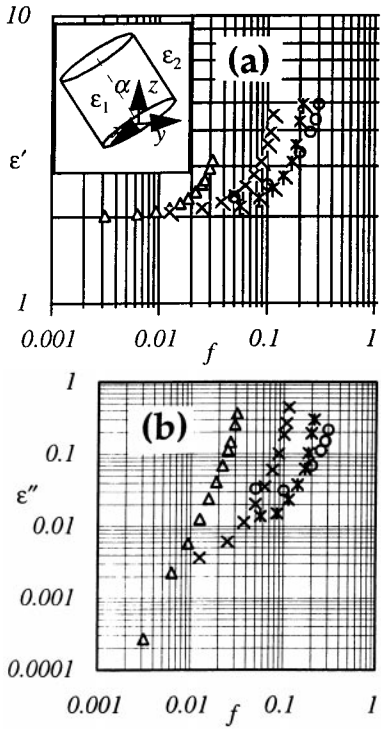

Fig. 10. (a) Same as in Figure 9a for the real part of the effective permittivity. The rod axis is oriented at 30° with respect to the electric field vector direction, *i.e.* the z-direction. (b) Same as in Figure 9b for the imaginary part of the effective permittivity.

given inclusion density and a given volume fraction, rods provide less surface area. On physical grounds, one expects that the more extended shape, that is by increasing the radius-to-length ratio r/l, which deviates from spherical provides what is needed for contact: they are characterized by more favorable depolarization factors. These issues have evident bearing on understanding a variety of observations concerning composites made of carbon fibers blended with epoxies and silicon elastomers [23].

4 Conclusion

The basic goal of the research described in this article has been to review a computational electrostatics approach of the dielectric properties of heterogeneous materials. Hence the basic definitions and the numerical procedure were briefly discussed. Due to space limitations we have only been able to touch on some of the unique aspects of dielectric properties of heterostructures. In the preceding sections we have shown that these materials can have a variety of electrical behaviors. Let us return to an issue raised in the Introduction. Because of the importance of the microstructure parameters in practice [24], the computational electrostatics approach that was described here provides a robust framework for calculating the "exact" effective permittivity of a wide variety of materials and will advance our understanding of the structure-property correlations in composite materials. Other examples involve the elastic, magnetic, thermal and diffusive properties of composite materials. Furthermore, the simulational data can be used to assess predictive theories for permittivity and conductivity.

The complexity of the electrical behavior of multicomponent composite material makes it theoretical and experimental study a great challenge. Many important questions remain unanswered. At this point it seems appropriate to consider what directions research in this field will take in the next few years. From our personal perspective, we clearly see a multitude of scientific challenges. The immediate focus is likely to go beyond the quasistatic approximation, that is to study the effect of frequency of the applied field in order to check explicitly theories aiming at elucidating the mechanisms of dielectric relaxation in these materials. This study was limited to the cases in which all the objects are periodically arranged in space. An interesting extension of our methodology is the simulation of the effective permittivity for realistic representations of the complex microstructure in model random composite media [25]. Also the conditions under which models of composite microstructure can account for the percolative characteristics observed need to be studied. These topics are currently being investigated.

From an engineering perspective, one would like to manipulate the morphology of these heterostructures so as to produce unusual device dielectric characteristics or further improve existing devices. For example, one of the greatest challenges for materials science is the creation of supramolecular materials in which the constituents are regular nanostructures. In seeking to address this question a more fundamental question is raised by consideration of the measurements, made by a variety of techniques, of the broadband dielectric spectrum. Application of recently developed methods, such as the resolution of a Fredholm equation using the Tikhonov regularization technique, provides an opportunity to achieve unique insight into polarization phenomena that occur in dielectric heterostructures [26].

The widespread natural occurrence of multiscale systems provides further motivation for research in this direction. We hope that this work inspires experimenters and theorists to attack some of the many problems in this exciting and challenging field. In short, there are rich opportunities for a continued impact of dielectric heterostructures in engineering, and the technological capabilities appear to be up the challenge.

The work described here is a result of important contributions from a number of researchers at the University of Brest and Centre de Génie Électrique de Lyon, France. Laboratoire d'Électronique et Systèmes de Télécommunications is Unité Mixte de Recherche CNRS 6616 and Centre de Génie Électrique de Lyon is Unité Propre de l'Enseignement Supérieur Associée CNRS 5005.

References

1. R. Landauer, in *Electric Transport and Optical Properties of Inhomogeneous Media*, edited by J.C. Garland, D.B. Tanner (AIP Conference Proceedings, No. 40, American Institute of Physics, New York, 1978), p. 2.
2. M. Sahimi, *Applications of Percolation Theory* (Taylor and Francis, London, 1994).
3. D. Stauffer, A. Aharoni, *Introduction to Percolation Theory*, 2nd edn. (Taylor and Francis, London, 1992).
4. D.J. Bergman, D. Stroud, Solid State Phys. **46**, 147 (1992).
5. *Progress in Electromagnetics Research: Dielectric Properties of Heterogenous Materials*, edited by A. Priou, (Elsevier, New-York, 1992) and references therein; see also for a recent review on electrical and optical properties, we refer to the Proceedings of the Second International Conference on Electrical and Optical Properties of Inhomogeneous Media (Physica A **157**, (1989)).
6. C. Brosseau, J. Appl. Phys. **75**, 672 (1994).
7. C. Brosseau, F. Boulic, C. Bourbigot, P. Queffelec, Y. Le Mest, J. Loaëc, A. Beroual, J. Appl. Phys. **81**, 882 (1997).
8. F. Boulic, C. Brosseau, Y. Le Mest, J. Loaëc, F. Carmona, J. Phys. D: Appl. Phys. **31**, 1904 (1998).
9. A.K. Jonscher, *Universal Relaxation Law* (Chelsea Dielectrics Press, London, 1997).
10. B. Sareni, L. Krahenbühl, A. Beroual, C. Brosseau, J. Appl. Phys. **80**, 1688 (1996).
11. B. Sareni, L. Krahenbühl, A. Beroual, C. Brosseau, J. Appl. Phys. **80**, 4560 (1996).
12. B. Sareni, L. Krahenbühl, A. Beroual, C. Brosseau, J. Appl. Phys. **81**, 2375 (1997).
13. A. Boudida, A. Beroual, C. Brosseau, J. Appl. Phys. **83**, 425 (1998).
14. C.A. Brebbia, *The Boundary Element Method for Engineers* (Pentech Press, London, 1980); see also O.C. Zienkiewicz, R.L. Taylor, *The Finite Element Method*, (McGraw-Hill, London, 1989), Vol. 1.
15. W.H. Press, B.P. Flannery, S.A. Teukolsky, W.T. Vetterling, *Numerical Recipes* (Cambridge University Press, New York, 1986).
16. R.C. McPhedran, D.R. McKenzie, Proc. R. Soc. Lond. A **359**, 45 (1978).
17. R. Tao, Z. Chen, P. Sheng, Phys. Rev. B **41**, 2417 (1989).
18. A. Sihvola, J.A. Kong, IEEE Trans. Geosci. Remote Sensing **26**, 420 (1988); see also A. Sihvola, J.A. Kong, IEEE Trans. Geosci. Remote Sensing **27**, 101 (1989).
19. C. Liu, L.C. Shen, J. Appl. Phys. **73**, 1897 (1993).
20. D.J. Bergman, Phys. Rep. **43**, 377 (1978); see also D.J. Bergman, Ann. Phys. **138**, 78 (1982); D.J. Bergman, J. Phys. C **12**, 4947 (1979).
21. G.W. Milton, J. Appl. Phys. **52**, 5286 (1981).
22. A. Boudida, A. Beroual, C. Brosseau, in *Proceedings of the Conference on Electrical Insulation and Dielectric Phenomena*, Atlanta, Georgia, USA, 1998, Vol. 1, pp. 261-264.
23. F. Carmona, F. Barreau, P. Delhaes, R. Conet, J. Phys. Lett. **41**, L531 (1980); see also F. Carmona, A. El Amarti, Phys. Rev. B **55**, 3284 (1987); I. Balberg, N. Binenbaum, Phys. Rev. B **28**, 3799 (1983); I. Balberg, C.H. Anderson, S. Alexander, N. Wagner, Phys. Rev. B **30**, 3933 (1984).
24. D.S. McLachlan, M. Blaszkiewicz, R.E. Newnham, J. Am. Ceram. Soc. **73**, 2187 (1990).
25. A.P. Roberts, M.A. Knackstedt, Phys. Rev. E **54**, 2313 (1996).
26. H. Schäfer, E. Sternin, R. Stannarius, M. Arndt, F. Kremer, Phys. Rev. Lett. **76**, 2177 (1996).